Response of a homeotropic nematic liquid crystal to rectilinear oscillatory shear

T. Börzsönyi and Á. Buka
Research Institute for Solid State Physics and Optics, Hungarian Academy of Sciences, P.O. Box 49, H-1525 Budapest, Hungary

A. P. Krekhov* and L. Kramer
Institute of Physics, University of Bayreuth, D-95440 Bayreuth, Germany

(Received 19 March 1998)

The response of a homeotropically aligned nematic liquid crystal layer to oscillatory rectilinear shear (Couette flow) was investigated for frequencies f between 0.01 and 200 Hz and layer thickness d between 10 and 130 μm. Below the onset of instability the cell was placed between crossed polars and light transmission was studied using a parallel light beam. The experimental results for the transmitted light intensity agree quantitatively with numerical solutions of the nematodynamic equations for different cell thicknesses, oscillation frequencies, and amplitudes. For frequencies between 25 and 150 Hz the critical oscillation amplitude for the onset of a spatial pattern, observed in polarized white light, could be reached. The pattern consisted of stationary rolls perpendicular to the direction of the oscillation. The experimentally obtained frequency dependence of the critical shear amplitude for the roll instability for different cell thicknesses is compared with an existing theory and the results of numerical calculations. [S1063-651X(98)09411-2]

PACS number(s): 61.30.Cz, 61.30.Gd, 64.70.Md, 47.20.−k

I. INTRODUCTION

Nematic liquid crystals (NLCs) exhibit interesting flow phenomena due to the coupling between the local molecular orientation (director $\hat{\mathbf{n}}$) and the velocity field $\mathbf{v}$. The flow properties of NLCs are characterized by Leslie viscosity coefficients $\alpha_1,\ldots,\alpha_6$, two of which $\alpha_2(<0)$ and α_3 are important in describing the coupling between flow and director orientation [1–4]. In the case of steady, plane, parallel shear flow, e.g., along the x axis with a velocity field $v_x(z)$ ($v_y=v_z=0$) and in the absence of other torques, the director will tend to align in the flow plane (x-z plane) at a fixed angle $\theta_{fl}=\pm\arctan(\alpha_3/\alpha_2)^{1/2}$ with the x axis if $\alpha_3<0$ (the $\pm$ sign pertains to positive/negative shear rate $\partial v_x/\partial z$). Negative α_3 is found in common nematics. In materials with $\alpha_3>0$, which occurs in particular near a nematic-smectic transition, instead of flow alignment there is a more complicated motion [5–7]. In the usual situation of a nematic layer sandwiched between confining plates at $z=\pm d/2$ the director is anchored at the boundaries and the hydrodynamic torques are countered by elastic torques. Then orientational instabilities can result (see, e.g., [4,8,9]).

Of particular interest have been flow phenomena in nematic layers where a steady rectilinear Couette flow is induced by moving one of the confining plates parallel to its plane in the x direction. The drawback of this situation is that an (approximately) steady state cannot be maintained experimentally for a long time. Here we are concerned with *oscillatory* rectilinear Couette flow where the velocity field $v_x(z,t)$ oscillates with a time average $\langle v_x\rangle=0$.

There are two quite different cases depending on whether the prealignment of the director is perpendicular to the flow plane, i.e., in the y direction, or within the flow plane. The first case has been clarified in classical experiments by Pieranski and Guyon [10,11] and theoretical work of Dubois-Violette and Manneville (for an overview see [9]). For NLCs with $\alpha_3<0$ one finds a transition to rolls oriented along the flow direction, which transforms into a homogeneous distortion when a stabilizing magnetic field is applied [11].

In the second case when the director is prealigned within the flow plane the dynamical behavior under oscillatory flow can be quite complex and has not been clarified completely.

First, one must consider the response of the system before any instability occurs (basic state) where the director generally oscillates around its equilibrium position induced by the boundaries. Beyond the small-amplitude linear regime one finds a response that is nonlinear in the shear strain. Up to this shear amplitude the temporal behavior of the director has been calculated for a specific frequency range using appropriate approximations [12,13].

In this frequency range the viscous penetration depth $\sqrt{\eta/\rho\omega}$, $\omega=2\pi f$, is much larger than the cell thickness d, where η is an appropriate effective shear viscosity and ρ denotes the NLC mass density (alternatively the inequality can be written in the form $\tau_v\omega\ll 1$, where $\tau_v=\rho d^2/\eta$ is the viscous damping time). Then the flow can be approximated by the simple linear Couette flow field, which amounts to neglecting the time derivative (inertia term) in the Navier-Stokes equation. This assumption applies also to the present work.

Next, one may consider Fréedericksz-type instabilities where the time-averaged director reorients homogeneously in the plane of the layer. For the simple linear Couette flow field no homogeneous instabilities are predicted to occur (in contrast to the case of Poiseuille flow) [14,15], even if the possibility of transitions out of the flow plane is included [15,16].

In fact, above a critical flow amplitude, transitions to spatially periodic roll states with period of the order of the cell

*Permanent address: Institute of Molecule and Crystal Physics, Russian Academy of Sciences, 450025 Ufa, Russia.

thickness have been observed in homeotropic (director perpendicular to the confining plates) [17–20] and planar alignment (director along the flow direction) [21,22]. In the experiments of Scudieri at ultrasonic frequencies (15 kHz) a transition to stationary rolls with the roll axis perpendicular to the flow was observed [17]. Subsequently, at low frequencies stationary rolls with the axis perpendicular or parallel to the flow, depending on the applied frequency, were observed [18]. A perpendicular stationary roll pattern was also observed by Guazzelli [19] at 500 Hz. Some other results about optically detected transitions at low frequencies without particular information on the evolving pattern (wave number and orientation) have also been published [20]. An approximate theoretical treatment for homeotropic alignment was presented by Kozhevnikov [23] and compared with the results of [20]. A similar treatment was done for planar alignment [21,22]. The investigation by Guazzelli was embedded in a study of instabilities resulting from elliptic shear flow [24–26], where a mechanism is operative that is understood quite well [27,28].

A transition to a state with broad, oblique traveling bands was observed by Clark *et al.* [12] for planar (at $\alpha_3>0$) and homeotropic alignment (for both signs of α_3). We are not aware of an explanation for this phenomenon.

In this paper we present a systematic, quantitative, experimental study of homeotropically oriented nematic layers subject to oscillatory rectilinear Couette flow covering a reasonable range of frequencies ($0.01\ \text{Hz}<f<200\ \text{Hz}$) and cell thicknesses ($10\ \mu\text{m}<d<130\ \mu\text{m}$). An investigation of the situation in the basic state, before any instabilities arise, is included since a thorough understanding and control of this situation are essential before proceeding to the onset of the roll instability.

Above the critical amplitude, which decreases with increasing frequency, we find stationary rolls oriented perpendicular to the flow plane with period of the order of the layer thickness. The bifurcations appear to be reversible. The threshold is compared with results obtained from a numerical evaluation of the hydrodynamic equations and with the only available analytic theory [23]. Whereas the agreement with the numerical results is good except in parameter ranges where the critical oscillation amplitude becomes large (in physical units), there is substantial deviation from the analytic theory.

In Sec. II the experimental setup is described. In Sec. III the experimental results are presented and discussed. Some conclusions and an outlook are given in Sec. IV.

II. EXPERIMENTAL SETUP

A nematic liquid crystal layer of thickness d is confined between two parallel horizontal glass plates (see Fig. 1) without a spacer. The lower plate is rigidly fixed to a brass block, which is adjustable in order to control the parallelism of the glass plates. This is done by observing the interference fringes in coherent visible light. By changing the tilt angle of the brass block one is able to have less than 2 fringes/cm, which means that the cell thickness varies about 0.5 μm/cm or even less. The temperature of the brass block is controlled by a thermostat with an accuracy of 0.1 °C.

The upper plate is attached to a steel rod that is guided by

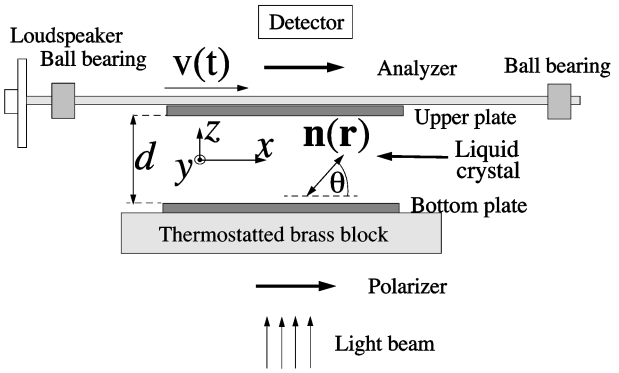

FIG. 1. Experimental setup.

two high-precision linear ball bearings. The maximum radial play of the ball bearings is 6 μm unloaded, but in our setup the ball bearings are preloaded, which gives us a maximum radial play below 3 μm.

One end of the metal rod is bound to the membrane of a loudspeaker (membrane diameter 24 cm) that is driven by the amplified signal of a signal generator. When using a sine excitation the displacement of the upper plate is ideally of the form $x(t)=A_x \sin \omega t$, where $\omega=2\pi f$. This is the case to a very good approximation for $f>20$ Hz. For $f<20$ Hz higher harmonics become noticeable, although with much smaller amplitudes. The angle between the plane of the upper glass plate and the metal rod is below $10'$. This tilt would cause a $\delta d/d=0.003$ during one period of the oscillation if $A_x=d$. This is negligible compared to the side movement caused by the radial play of the ball bearings.

The cell thickness could be varied by changing the vertical position of the brass block. The extrapolated position corresponding to zero thickness could be determined with an accuracy $\approx \pm 2\ \mu$m. Once the zero point was determined one could vary the cell thickness with an accuracy of $\pm 0.2\ \mu$m with respect to it.

Below the onset of instability the transmitted light intensity was measured by a semiconductor detector using parallel light (source: diode laser, wavelength $\Lambda=670$ nm) between crossed polarizers. The spatial patterns occurring at higher amplitude were observed in transmitted polarized white light (without analyzer) and detected by a charge coupled device camera. The images were recorded onto video tape.

The motion of the upper plate was monitored by two independent methods.

(i) The displacement in the x and one more (y or z) direction was detected by a one-dimensional semiconductor position-sensitive detector. This detector provides continuous position data of a light spot traveling over its surface. Using a laser diode as the illumination source, we have after amplification a signal that is roughly 0.2 V/μm. It allows us to measure the position of the upper plate with an accuracy of $\pm 0.2\ \mu$m. This can be improved by using a focused, more intensive light spot and more carefully depressed noise.

(ii) The acceleration of the upper plate was measured with piezoelectric accelerometers in all three directions (x, y, and z). A piezoelectric accelerometer is mainly sensitive in one specific direction with a maximum transverse sensitivity of 2–3%. Using three accelerometers, directed perpendicular to each other and parallel to the axes of our coordinate system,

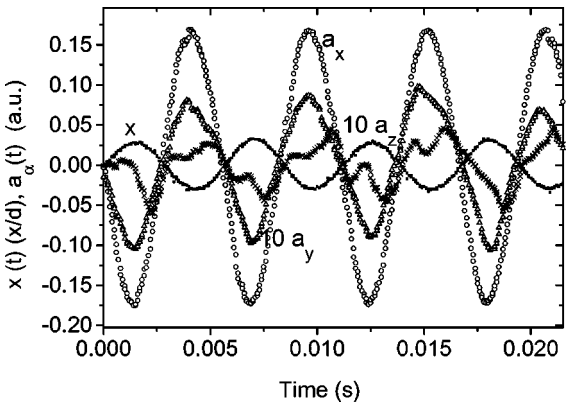

FIG. 2. Displacement of the upper plate $x(t)$ (□), measured by the position-sensitive photodetector and the acceleration of the upper plate in all three directions a_x (○) [a_y (△) and a_z (×) are multiplied by a factor of 10] measured with the piezoaccelerometers as a function of time. The frequency $f=186$ Hz, the cell thickness $d=50$ μm, and the oscillation amplitude $A_x=1.4$ μm.

one gets the signals a_x, a_y, and a_z from which the ratio of the transverse acceleration could be determined. These ratios, which we call ellipticities ($\epsilon_y=a_y/a_x$ and $\epsilon_z=a_z/a_x$), are easier to measure at higher frequencies since the acceleration is proportional to f^2.

Signals for a typical motion are shown in Fig. 2. The different curves correspond, respectively, to the displacement $x(t)$ of the upper plate measured with the one-dimensional position detector and the acceleration values $a_x(t)$, $10a_y(t)$, and $10a_z(t)$. By calculating the ratios of the maxima of the accelerations in the different directions one obtains the ellipticities $\epsilon_y=0.06$ and $\epsilon_z=0.03$ for this case. Alternatively, if one first calculates the Fourier spectrum of the acceleration signals and determines the ellipticity from the ratios of only the first harmonics one gets for the same measurements $\epsilon_{y1}=a_{y1}/a_x=0.05$ and $\epsilon_{z1}=a_{z1}/a_x=0.02$. The same ratios for the side movement were detected with the position-sensitive detectors at smaller frequencies and larger amplitudes.

In all of our experiments ϵ_{y1} and ϵ_{z1} were less than 0.07 and in many cases they were in the range of the error of the piezoaccelerometers (maximum transverse sensitivity). The origin of the side movement is on the one hand the radial play of the ball bearings and on the other hand the mechanical resonances of the setup at its eigenfrequencies. During the measurements we avoided mechanical resonances by choosing appropriate frequencies of the oscillation because a possible oscillation in the z direction would cause a Poiseuille component in the flow making the situation much more complicated.

The substance K15 [or 4-n-pentyl-4′-cyanobiphenyl (5CB)] was used for investigation. It has a nematic phase between 22.4 °C and 34.5 °C. The Leslie coefficient α_3 of 5CB is negative in the whole temperature range, which means that in steady flow at large flow gradients one has flow alignment. In the experiments the temperature was kept at $T=25$ °C. By using float glass plates a homeotropic initial alignment was achieved, which was checked between rotating crossed polars.

III. RESULTS AND DISCUSSION

A. Basic state

In order to gain confidence in the results for the instability (to be discussed subsequently) we first set out to reach quantitative agreement between the experiments for the basic state and the results of numerical solution of the standard set of nematodynamic equations [3,16]. From an analysis of the underlying hydrodynamic problem one expects the director to oscillate within the flow plane (see also the Appendix). Then the experimental signal, i.e., the transmitted light intensity I_{Tr} between crossed polars, should be related to the calculated director angle θ_0 (measured from the x axis):

$$I_{Tr}=I_0 \sin^2 2\alpha \sin^2\frac{\Phi}{2}, \quad \Phi=\frac{2\pi}{\Lambda}\int_{-d/2}^{d/2}\Delta n\, dz, \qquad (1)$$

where Λ is the wavelength of the light. The angle α between the x direction and the polarization of the incident light is kept at 45°. The birefringence is given by

$$\Delta n=n_\perp\left(1-\frac{n_\parallel^2-n_\perp^2}{n_\parallel^2}\cos^2\theta_0\right)^{-1/2}-n_\perp, \qquad (2)$$

where $n_\parallel$ and $n_\perp$ are the refractive indices for light with polarization parallel and perpendicular to the director, respectively. One can see that the maximum transmitted intensity is $I_{max}=I_0$.

The experiments were carried out for different cell thicknesses in the range $10\ \mu\text{m}<d<70\ \mu\text{m}$. We measure the displacement of the upper plate in dimensionless units $x(t)/d$, while the transmitted light intensity I_{Tr} measured between crossed polars is normalized by its maximum value I_{max} (see above).

In Figs. 3(a)–3(d) the experimental data for the normalized transmitted light intensity versus time are plotted for $f=42.5$ Hz, $d=52$ μm, and four values of A_x/d. Also shown is the normalized upper-plate displacement, which is in this range of frequency accurately described by $x(t)/d=(A_x/d)\sin\omega t$. The continuous lines are theoretical curves evaluated from the nematodynamic equations using material parameters for 5CB (see the Appendix). One can see that at this frequency the maximum of the intensity of the transmitted light coincides with the maximum of the upper plate's displacement in time (no phase shift). This is typical for the range where the elastic terms are irrelevant in the director equation, i.e., when $\epsilon=1/(\tau_d\omega)\ll 1$ (here $\tau_d=\gamma_1 d^2/K_{11}$ is the director relaxation time and $\epsilon\approx 10^{-3}$).

Comparing Figs. 3(a) and 3(b) one sees that a rather small increase of the amplitude can induce a remarkable increase in the intensity of the optical signal, in agreement with the results of the calculations. Above a certain amplitude [see Fig. 3(c)] the maximum path difference Φ [see Eq. (1)] exceeds π. Then the maximum of the optical signal splits up in time into two peaks and at significantly larger amplitudes shows oscillatory behavior [Fig. 3(d)]. We note good quantitative agreement between experiment and theory without any fitting parameters in numerical simulations.

In Fig. 4 the normalized transmitted light intensity detected at the time of maximum displacement of the upper plate is plotted as a function of the reduced amplitude A_x/d

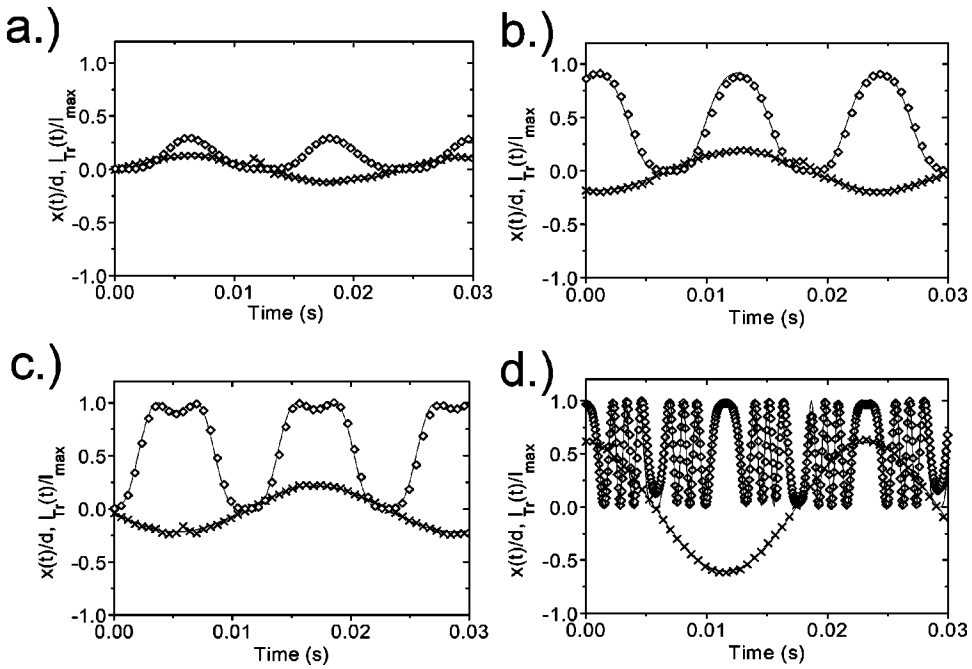

FIG. 3. Normalized displacement of the upper plate $x(t)/d$ (crosses) and the normalized transmitted light intensity $I_{Tr}(t)/I_{max}$ (diamonds) between crossed polars plotted as a function of time for the amplitudes (a) $A_x/d=0.11$, (b) $A_x/d=0.18$, (c) $A_x/d=0.22$, and (d) $A_x/d=0.63$. The frequency of oscillatory flow $f=42.5$ Hz and the cell thickness $d=52$ μm. The continuous lines are calculated from the standard set of nematodynamic equations [3,16] using 5CB material parameters.

for the same parameters as in Fig. 3 and compared with the results of nematodynamic equations simulations. As expected, the optical signal generally oscillates between 0 and 1. However, when approaching the onset of the pattern formation (in this case $A_{xc}/d\approx 1$) the hydrodynamic instability develops at some locations in the cell, which can be observed by the decrease of the maxima and increase of the minima of the optical signal.

In Fig. 5 the behavior at low frequency is demonstrated. The normalized transmitted light intensity and upper-plate displacement versus time are shown for $d=44$ μm and $f=0.1$ Hz, where $\epsilon=0.6$ and the amplitude was fairly small: $A_x/d=0.2$. At this frequency, as mentioned before, the displacement curve $x(t)$ is quite anharmonic. The positions of the extrema of $x(t)$ and the maximum of $I_{Tr}(t)$ clearly display a phase shift between the upper-plate displacement and the optical response. This results from the influence of the elastic terms in the director dynamic equation. The experimental results are compared with full numerical solutions of nematodynamic equations (including elastic terms), represented by continuous lines in the figure.

In Fig. 6 measurements of the phase shift, (the phase shift equals 0 if the maxima of the transmitted light intensity coincide with the extrema of the displacement in time and ± 1 if its maxima coincide with the zero points of the displacement) versus frequency are presented for three cell thicknesses. The amplitude A_x was around 7 μm in the high-frequency regime, while at small frequencies ($f<0.1$ Hz) larger amplitudes were needed up to $A_x\approx 20$ μm in order to obtain the same optical intensity. One clearly sees the transition from the elasticity dominated regime occurring at very low frequency, where the phase shift is -1, to the high-frequency regime with vanishing phase shift.

The maximum of the transmitted intensity, which for small amplitudes is obtained at the moment of maximum distortion of the director ($\Phi<\pi$), was measured as a function of the frequency for various values of A_x/d. In Fig. 7 the normalized transmitted intensity is shown for $A_x/d=0.14$. The continuous curve corresponds again to direct numerical simulations of the nematodynamic equations.

We note that the good agreement between experimental data and numerical result (as presented above) justifies the prediction that $n_y=0$ (no out-of-plane motion) [15,16]. This agreement could be achieved for $d\leqslant 70$ μm up to an ampli-

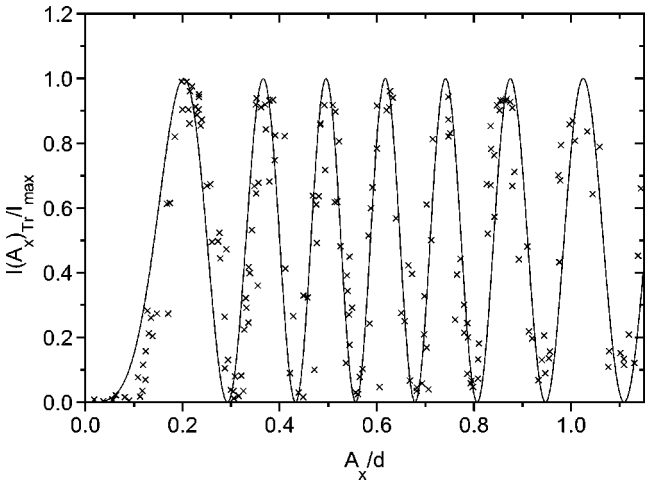

FIG. 4. Normalized transmitted intensity $I(A_x)_{Tr}/I_{max}$ at the moment of maximum displacement of the upper plate plotted as a function of the oscillation amplitude A_x/d (crosses). Otherwise the parameters are the same as in Fig. 3. The continuous line is calculated from nematodynamic equations using 5CB material parameters.

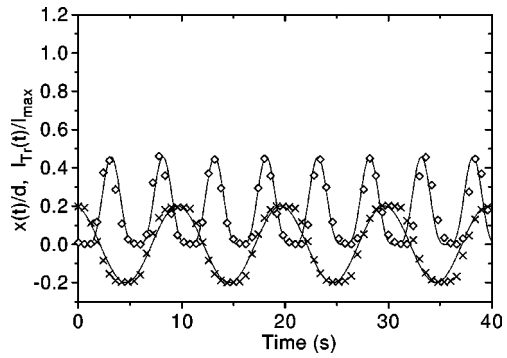

FIG. 5. Normalized displacement of the upper plate $x(t)/d$ (crosses) and the normalized transmitted light intensity $I_{Tr}(t)/I_{max}$ (diamonds) between crossed polars plotted as a function of time for the amplitudes $A_x/d=0.2$. The flow frequency $f=0.1$ Hz and the cell thickness $d=40$ μm. The continuous lines are calculated using 5CB material parameters.

tude $A_x/d \leqslant 1$ or $A_x \leqslant A_{xc}$ (whichever occurred first). Otherwise discrepancies developed.

B. Onset of the roll structure

When increasing A_x at the fixed frequency, above a critical value (A_{xc}) one observes the onset of a stationary pattern. The pattern consists of rolls with their axes normal to the oscillation direction. It is observable in white polarized light (see Fig. 8 as an example).

The threshold amplitude (A_{xc}) has been determined precisely at several frequencies by the following method. The driving voltage of the loudspeaker was increased slowly (controlled by computer) until the pattern had developed; then it was decreased to the starting value. The oscillation amplitude of the upper plate was detected and the corresponding images were recorded and analyzed. The contrast was defined to be the root mean square of the variations of the intensity in a chosen horizontal line. The contrast as a function of the oscillation amplitude is plotted in Fig. 9. The two symbols correspond to increasing and decreasing amplitudes, respectively. The curves appear continuous and no hysteresis was observed. Consequently, linear stability

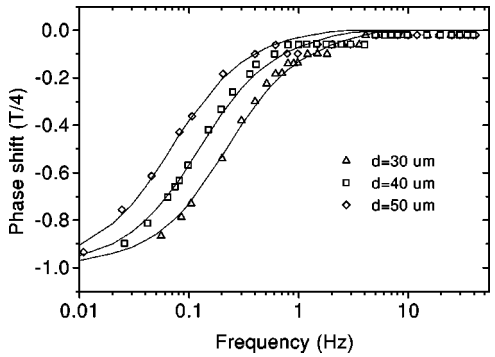

FIG. 6. Phase shift between the upper plate oscillation and the transmitted intensity as a function of frequency. The data were measured for cell thicknesses $d=30$, 40, and 50 μm. The continuous lines correspond to the simulations of nematodynamic equations. The steps observed at $f=1$, 2, and 5 Hz in the experimental data originate from the data processing.

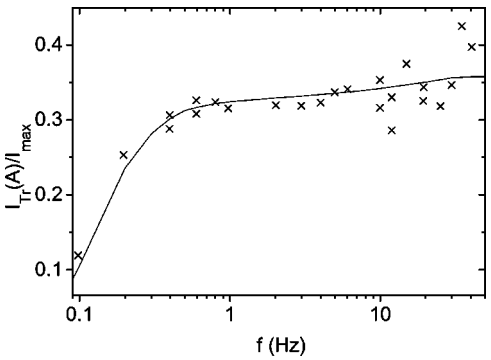

FIG. 7. Maximum value of the transmitted light intensity normalized to I_{max} as a function of the flow frequency for cell thickness $d=44$ μm and displacement amplitude $A_x/d=0.14$. The theoretical curve is obtained from the full numerical simulation of the nematodynamic equations.

analysis should be applicable for the determination of the threshold.

We mention that at some frequencies in the range 45 Hz $<f<80$ Hz we observed tilted rolls as well as nonstationary patterns consisting of traveling rolls. In these cases the ellipticity of the motion (ϵ_y and ϵ_z) was observed to be slightly larger than usual, probably due to mechanical resonances of the setup.

The experiment was carried out for cell thicknesses in the range 30 μm$<d<$130 μm. The threshold amplitude A_{xc} as a function of the frequency f is shown in Fig. 10(a). The different data correspond to thicknesses in the above range. As one can see in Fig. 10(a), the threshold increases rapidly with decreasing frequency. In Fig. 10(b) the same data are plotted in the form of A_{xc}/d versus d with the frequency as a parameter. Finally, in Fig. 11 we plot the data in the form suggested by the scaling law $A_{xc}/d=F(\tau_d\omega)$ with some

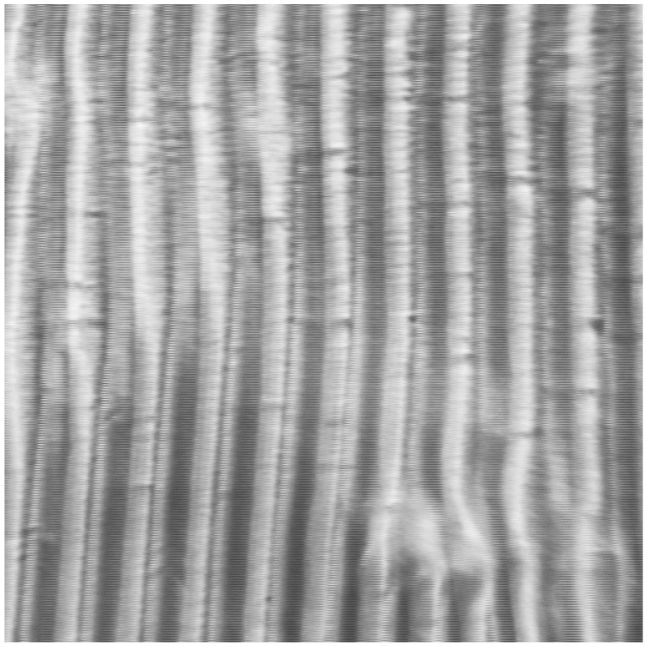

FIG. 8. Roll pattern observed in polarized white light at $f=40$ Hz and $A_x/d=0.7$. The rolls are perpendicular to the direction of the upper plate oscillations.

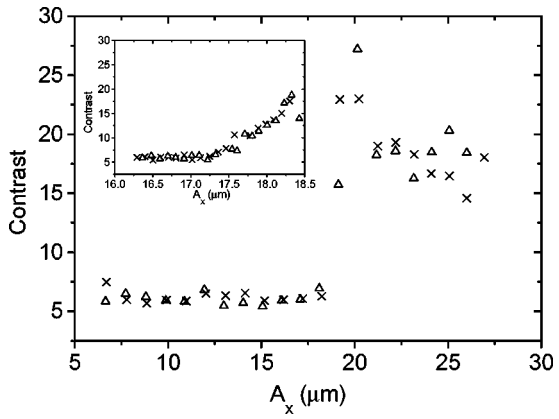

FIG. 9. Contrast of the images observed in polarized light at increasing (×) and decreasing (△) oscillation amplitude. The frequency was $f=127$ Hz, while the cell thickness $d=90$ μm.

function F. This scaling property can be read off the nematodynamic equations. Also included in Fig. 11 are the results of Ref. [23] (dashed line) as well as numerical results on the linear stability analysis of the basic state obtained by neglecting the inertia term in the nematodynamic equations (dotted line) (see the Appendix). Whereas there are substantial discrepancies between experiment and the results of Ref. [23], the agreement with the numerical simulations is actually

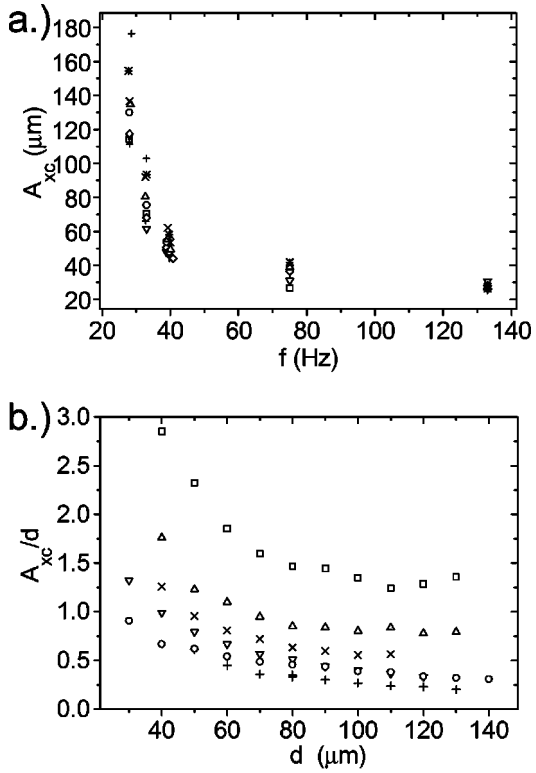

FIG. 10. (a) Threshold amplitude A_{xc} for the formation of the roll pattern as a function of the frequency f for cell thicknesses $d=40$ μm (□), $d=50$ μm (▽), $d=60$ μm (−), $d=70$ μm (|), $d=80$ μm (◇), $d=90$ μm (○), $d=100$ μm (△), $d=110$ μm (×), $d=120$ μm (*), and $d=130$ μm (+). (b) Normalized threshold amplitude A_{xc}/d as a function of the cell thickness for different frequencies: $f=28$ Hz (□), $f=33$ Hz (△), $f=38$ Hz (×), $f=40$ Hz (▽), $f=75$ Hz (○), and $f=133$ Hz (+).

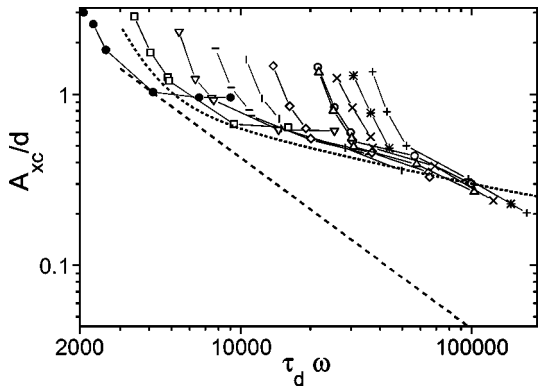

FIG. 11. Normalized threshold amplitude A_{xc}/d for the formation of the roll pattern as a function of the quantity $\tau_d\omega$ for cell thickness $d=30$ μm (●), $d=40$ μm (□), $d=50$ μm (▽), $d=60$ μm (−), $d=70$ μm (|), $d=80$ μm (◇), $d=90$ μm (○), $d=100$ μm (△), $d=110$ μm (×), $d=120$ μm (*), and $d=130$ μm (+). The dotted line corresponds to the numerical results of the linear stability analysis with fully rigid boundary conditions, while the dashed line is calculated from [23].

quite good, including the scaling behavior, except for low frequencies in thick samples. This corresponds to the case of large oscillation amplitudes (in physical units). The discrepancies are discussed in Sec. IV. At low frequencies (f below about 25 Hz) no periodic roll structure is observed; instead, at large amplitudes (when one would expect the formation of rolls) irregular patterns appear. Above 150 Hz the attainable maximum amplitude of the loudspeaker was not enough for the development of a spatial pattern. When going to small thicknesses ($d\approx 30$ μm and below) the contrast of the roll pattern diminishes, thus making threshold measurements difficult.

Concerning the wave number q_c of the roll pattern at threshold, we find experimentally an approximately constant value $q_c d/\pi\sim 1$ in the frequency range investigated (see Fig 12). From our simulations follows a very weak frequency dependence for the critical wave number q_c and $q_c d/\pi \sim 0.8$, whereas [23] predicted $q_c d/\pi\sim 0.5$.

IV. CONCLUDING REMARKS AND PERSPECTIVE

With regard to the basic state before the onset of instability, we may emphasize that considerable effort had to be put

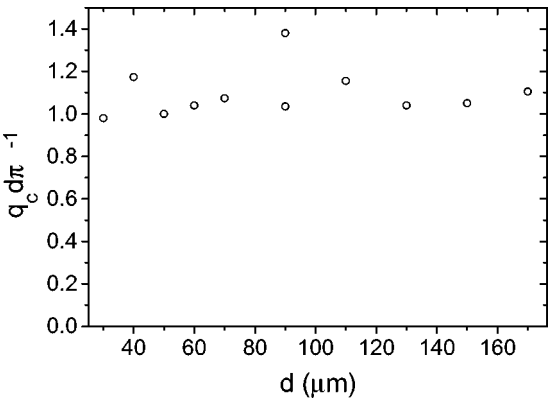

FIG. 12. Wave number of the roll pattern as a function of the cell thickness.

into optimizing the experiment before the quantitative agreement with theory as reported here could be achieved. This optimization was a prerequisite for capturing the roll threshold quantitatively.

We suspect that deviations from the ideal rectilinear flow excitation, which become relevant at large amplitude, are responsible for the remaining discrepancies. An indication for this conjecture is the discrepancy arising already subcritically in the basic flow (see the end of Sec. III A). Even a rather small z component of the motion of the upper plate may excite a substantial uncontrolled Poiseuille flow, which could lead to out-of-plane motion of the director. This would presumably delay the roll instability, as observed.

When trying to assess the theoretical situation it is useful to make a connection with the *elliptically* sheared case [19,24–26]. There one has satisfactory agreement with an approximate analytic stability analysis of the basic state [27,28]. The approximations mainly involve a time-averaging procedure that can be rephrased in terms of a lowest-order time Fourier expansion and a one-mode approximation with simple symmetry of the z dependence. The mechanism does not involve the inertia term, so it was discarded in the analysis. The threshold condition is of the form $X_c Y_c / d^2 \sim (\tau_d \omega)^{-1}$, where X_c and Y_c are the critical oscillation amplitudes in the two directions. Clearly in the limit where one amplitude becomes small, the critical amplitude for the other diverges. Therefore, this mechanism does not lead to a threshold for rectilinear shear, so here a different mechanism is needed.

In the case of *rectilinear* shear employing a somewhat similar approximation scheme for the linear stability analysis as was used for the elliptic case, but not dropping the inertia term, Kozhevnikov [23] arrived at a threshold $A_c/d \sim [(\tau_d \tau_v)^{1/2} \omega]^{-1}$. It diverges when the viscous dissipation time is set to zero, i.e., when the inertia term is dropped. The approximations made involve, in particular, a small-amplitude approximation of the basic state, a lowest-order time Fourier approximation, a one-mode approximation with simple symmetry for the z dependence, and neglect the elastic torque in the oscillatory part of the destabilizing fluctuations. Then one can see that a mechanism for instability giving a time-averaged destabilizing torque on the director is indeed provided through the phase shift between the basic state velocity oscillations and the oscillatory part of the velocity fluctuations, induced by the inertia term in the Navier-Stokes equation (without the phase shift the relevant time averages are zero). However, another source of a time-averaged torque is provided by the elastic terms, which are effective in a boundary layer of thickness $(\tau_d \omega)^{-1/2}$. Unfortunately, a one-mode approximation does not capture this effect and therefore an analytic treatment is difficult. Nevertheless, it is clear that the latter mechanism becomes important at low frequencies. The results of [23] do not describe our experimental data. On the other hand, the agreement between experiment and a numerical stability analysis is actually quite good. Where the experimental data deviate from that theory, they violate an analytic scaling property. We tentatively conclude that the approximations made in the analytic theory are not valid at the low frequencies considered here.

From a more general point of view the mechanism leading to the roll instability involves the following aspect. We are dealing with a system that is parametrically driven in a time-periodic and, when inertia terms are neglected, essentially spatially *homogeneous* manner (the velocity gradient of the basic flow, which is the relevant quantity, is spatially constant). Then, as long as the state remains homogeneous, the spatial coupling of the director through orientational diffusion is not activated. The system behaves as a zero-dimensional one, which is integrable and cannot develop instabilities. The only way to produce a time-averaged torque on the director is to establish (spontaneously) a space dependence, thereby activating the spatial coupling (and escape integrability). A positive growth rate of spatial fluctuations is then possible. Thus, paradoxically, the diffusive coupling is instrumental in producing the spatial inhomogeneities. The effect is complementary to the mechanism operative when the driving is *inhomogeneous* (as in Poiseuille flow) and the director undergoes a *homogeneous* transition [14–16].

Although our results represent a substantial advance over previous studies of this problem they leave room for improvement. In the future we hope to develop an analytic (or semianalytic) approach to capture the essential features of the numerical results presented here. Hopefully our investigation can be extended to include ellipticity of the shear so that the crossover to that domain can finally be clarified. We are currently working on an experimental apparatus that allows us to apply a controlled ellipticity of the shear in order to approach the crossover experimentally. To our knowledge, this crossover has been observed only in one experiment for $d = 50$ μm and $\omega = 500$ Hz [19].

ACKNOWLEDGMENTS

We thank N. Éber for fruitful discussions on technical problems and W. Pesch and O. Tarasov for fruitful discussions on computational problems. A.K. is grateful to the Alexander von Humboldt Stiftung for financial support and, together with A.B., wishes to acknowledge the hospitality of the University of Bayreuth. B.T. wishes to thank the Bashkir State University and the Institute of Molecule and Crystal Physics (Ufa) for their hospitality and A.K. wishes to acknowledge the hospitality of the Research Institute for Solid State Physics (Budapest). Financial support from VW Stiftung, EU Network No. ERB FMR XCT 960085, MTA Grant No. OTKA T014957, DFG Grant No. Kr 690/12-1, and INTAS Grant No. 96-498 is gratefully acknowledged.

APPENDIX: NUMERICAL SIMULATIONS

A previous study of the uniform response (i.e., no x and y dependence) under oscillatory rectilinear Couette flow shows that the director oscillates within the flow plane (x-z plane) without out-of-plane instabilities [15,16]. Allowing for periodic modulations of the director and the velocity along x one can write

$$n_x = \cos\,\theta(x,z,t), \quad n_y = 0, \quad n_z = \sin\,\theta(x,z,t),$$
$$v_x = v_x(x,z,t), \quad v_y = 0, \quad v_z = v_z(x,z,t). \tag{A1}$$

Then the standard nematodynamic equations [3,4] assume the form (the notation $f_{,i} = \partial_i f$ has been used throughout)

$$\gamma_1\Big[n_z n_{x,t}-n_x n_{z,t}+n_z(\mathbf{v}\cdot\boldsymbol{\nabla})n_x-n_x(\mathbf{v}\cdot\boldsymbol{\nabla})n_z - \frac{1}{2}(v_{x,z}-v_{z,x})\Big]+\gamma_2\Big[n_x n_z(v_{x,x}-v_{z,z})+(n_z^2-n_x^2)\times\frac{1}{2}(v_{x,z}+v_{z,x})\Big]$$
$$=K_{11}[n_z\partial_x(\boldsymbol{\nabla}\cdot\hat{\mathbf{n}})-n_x\partial_z(\boldsymbol{\nabla}\cdot\hat{\mathbf{n}})] +K_{33}[n_z\partial_z(n_{x,z}-n_{z,x})+n_x\partial_x(n_{x,z}-n_{z,x})], \tag{A2}$$

$$\rho[v_{x,t}+(\mathbf{v}\cdot\boldsymbol{\nabla})v_x]=-p_{,x}+\sigma_{xx,x}+\sigma_{zx,z},$$
$$\rho[v_{z,t}+(\mathbf{v}\cdot\boldsymbol{\nabla})v_z]=-p_{,z}+\sigma_{xz,x}+\sigma_{zz,z}, \tag{A3}$$

with the components of the stress tensor

$$\sigma_{xx}=-K_{11}(\boldsymbol{\nabla}\cdot\hat{\mathbf{n}})n_{x,x}+K_{33}(n_{x,z}-n_{z,x})n_{z,x}\alpha_1 A n_x^2 +(\alpha_2+\alpha_3)n_x N_x+\alpha_4 v_{x,x}+(\alpha_5+\alpha_6)n_x \times\Big[n_x v_{x,x}+n_z\frac{1}{2}(v_{x,z}+v_{z,x})\Big], \tag{A4}$$

$$\sigma_{zx}=-K_{11}(\boldsymbol{\nabla}\cdot\hat{\mathbf{n}})n_{z,x}-K_{33}(n_{x,z}-n_{z,x})n_{x,x}+\alpha_1 A n_x n_z +\alpha_2 n_z N_x+\alpha_3 n_x N_z+\alpha_4\frac{1}{2}(v_{x,z}+v_{z,x})+\alpha_5 n_z\Big[n_x v_{x,x} +n_z\frac{1}{2}(v_{x,z}+v_{z,x})\Big]+\alpha_6 n_x\Big[n_x\frac{1}{2}(v_{x,z}+v_{z,x})+n_z v_{z,z}\Big],$$

where

$$A=n_x^2 v_{x,x}+n_z^2 v_{z,z}+n_x n_z(v_{x,z}+v_{z,x}),$$
$$N_x=n_{x,t}+(\mathbf{v}\cdot\boldsymbol{\nabla})n_x-\frac{1}{2}n_z(v_{x,z}-v_{z,x}), \tag{A5}$$
$$N_z=n_{z,t}+(\mathbf{v}\cdot\boldsymbol{\nabla})n_z-\frac{1}{2}n_x(v_{z,x}-v_{x,z}).$$

The components σ_{xz},σ_{zz} can be obtained by exchanging of the indices x and z in the expressions (A4) for σ_{zx} and σ_{xx}, respectively. In addition, one has the director normalization equation and the incompressibility condition

$$n_x^2+n_z^2=1, \quad v_{x,x}+v_{z,z}=0. \tag{A6}$$

Equations (A2)–(A6) are to be supplemented by the boundary conditions

$$\theta(z=\pm d/2)=\pi/2,$$
$$v_x(z=-d/2)=0, \quad v_x(z=d/2)=A_x\omega\cos\omega t, \tag{A7}$$
$$v_z(z=\pm d/2)=0, \quad v_{z,z}(z=\pm d/2)=0,$$

For sufficiently small shear amplitudes the system remains in a state that retains all the symmetries compatible with the external constraints, i.e., no x dependence and $v_z=0$ (from incompressibility). Then one has for the basic state $\theta=\theta_0(z,t)$, $v_x=v_{0x}(z,t)$ from Eqs. (A2) and (A3)

$$\gamma_1\theta_{0,t}-(\alpha_2\sin^2\theta_0-\alpha_3\cos^2\theta_0)v_{0x,z} =(K_{11}\cos^2\theta_0+K_{33}\sin^2\theta_0)\theta_{0,zz} +(K_{33}-K_{11})\sin\theta_0\cos\theta_0\theta_{0,z}^2, \tag{A8}$$

$$\rho v_{0x,t}=\partial_z\Big\{-(\alpha_2\sin^2\theta_0-\alpha_3\cos^2\theta_0)\theta_{0,t} +\frac{1}{2}[\alpha_4+(\alpha_5-\alpha_2)\sin^2\theta_0+(\alpha_3+\alpha_6 +2\alpha_1\sin^2\theta_0)\cos^2\theta_0]v_{0x,z}\Big\}. \tag{A9}$$

The direct numerical simulations of Eqs. (A8) and (A9) with boundary conditions (A7) were performed. In the frequency range $\omega\ll 1/\tau_v$ to be considered here ($\tau_v=\rho d^2/\gamma_1$ so that for $\rho\approx 10^3$ kg/m^3, $d\approx 10^{-4}$ m, and $\gamma_1\approx 10^{-1}$ N s/m^2 one has $1/\tau_v\approx 10^4$ s^{-1}) we found essentially no difference if the inertia term ($\rho v_{0x,t}$) was dropped in Eq. (A9). Omitting also the elastic coupling terms on the right-hand side of Eq. (A8) one can easily find

$$\theta_0(t)=\frac{\pi}{2}-\arctan\Big\{\frac{1}{\sqrt{\lambda}}\tanh\Big[\frac{\sqrt{\lambda}}{1-\lambda}a\sin\omega t\Big]\Big\},$$
$$v_{0x}(z,t)=a\omega\Big(z+\frac{d}{2}\Big)\cos\omega t, \tag{A10}$$

where $a=A_x/d$, $\lambda=\alpha_3/\alpha_2$, and the director is independent of z [12,16]. For torque-free boundary conditions [$\theta_{0,z}(z=\pm d/2)=0$] Eq. (A10) is in fact an exact solution of Eqs. (A8) and (A9) with the inertia term dropped. For strong anchoring [$\theta_0(z=\pm d/2)=\pi/2$] the elastic terms generate boundary layers of thickness $\sqrt{1/\tau_d\omega}$ (in physical units $\sqrt{K_{11}/\gamma_1\omega}$), which corresponds to the orientational diffusion length, which is neglected here. This is valid for the condition $\sqrt{1/\tau_d\omega}\ll 1$, i.e., $\omega\gg 1/\tau_d$ ($\tau_d=\gamma_1 d^2/K_{11}$ and for $\gamma_1\approx 10^{-1}$ N s/m^2, $d\approx 10^{-4}$ m, and $K_{11}\approx 10^{-11}$ N one has $1/\tau_d\approx 10^{-2}$ s^{-1}). The approximate solution (A10) is applicable for frequencies $1/\tau_d\ll\omega\ll 1/\tau_v$.

For the linear stability analysis of the basic state we linearize Eqs. (A2)–(A6) around the solution (A10)

$$\theta=\theta_0(t)+\theta_1(x,z,t),$$
$$v_x=v_{0x}(z,t)+v_{1x}(x,z,t), \quad v_z=v_{1z}(x,z,t) \tag{A11}$$

with small perturbations θ_1,v_{1x},v_{1z}. The pressure perturbation is eliminated by cross differentiation of the x and z components of the Navier-Stokes equation (A3) and v_{1x} is eliminated by the incompressibility condition. One is then left with two (rather lengthy) linear equations for the variables θ_1,v_{1z} with the coefficients depending on the basic solution θ_0,v_{0x}. The boundary conditions for the director and velocity perturbation are

$$\theta_1(z=\pm d/2)=0, \tag{A12}$$

$$v_{1z}(z=\pm d/2)=0, \quad v_{1z,z}(z=\pm d/2)=0.$$

From Floquet's theorem follows the general form of the solution of our linear problem

$$[\theta_1(x,z,t),v_{1z}(x,z,t)]=e^{\sigma t}e^{iqx}\sum_{m=-\infty}^{\infty}[b_m(z),c_m(z)]e^{im\omega t} + \text{c.c.}, \tag{A13}$$

where q is the wave number in the x direction. The coefficients $[b_m(z),c_m(z)]$ are expanded in a complete set of orthogonal functions that satisfy the boundary conditions (Galerkin method; see, e.g., [29]). We used a set of trigonometric functions for the angle $[b_m(z)]$ and Chandrasekhar functions for the velocity $[c_m(z)]$ [30]. After a projection procedure and truncation of time series and z modes one obtains a linear system for the expansion coefficients. Its solvability condition gives the growth rate function $\sigma(q,a)$. The condition $\mathrm{Re}[\sigma(q,a)]=0$ yields as usual the neutral curve $a_0(q)$. The threshold is given by $a_c=\min_q a_0(q)$, which also yields the critical wave number q_c for the pattern.

The calculations show that one has at threshold $\mathrm{Im}(\sigma)=0$, i.e., the bifurcation has a stationary character. Beyond threshold there are nonzero time averages $\langle\theta_1\rangle$ and $\langle v_{1z}\rangle$ corresponding to a stationary spatial modulation of the director and velocity in the form of a periodic roll structure. We have tested the error of the critical oscillation amplitude a_c by changing the order of truncation of the Galerkin expansion [Eq. (A13)]. We chose a sufficient number of time and z modes in the Galerkin expansion to restrict the relative error of the threshold a_c to well below 10^{-2}.

Since the basic state solution (A10) pertains to torque-free boundary conditions, we checked its stability also for those boundary conditions $\theta_{1,z}(z=\pm d/2)=0$. This was found to lead to a small decrease of the critical amplitude a_c. The reduction increased with decreasing frequency from $\sim 4\%$ at $\tau_d\omega=10^5$ to $\sim 8\%$ at $\tau_d\omega=10^3$. We have also tested the influence of the inertia term $\rho v_{i,t}$ in the Navier-Stokes equation for the perturbations. In the frequency range $1/\tau_d \ll \omega \ll 1/\tau_v$ considered here, where the basic state solution (A10) is valid, inclusion of the inertia term leads to a small decrease of a_c. The reduction was about 2% at $\omega \approx 0.2\tau_v^{-1}$ ($\tau_d\omega\approx 10^5$ in Fig. 11) and decreased with decreasing frequency.

The numerical computations were carried out for the following 5CB material parameters at 26 °C [31,32]: elasticity coefficients in units of 10^{-12} N, $K_{11}=5.95$, $K_{22}=3.77$, and $K_{33}=7.86$; viscosity coefficients in units of 10^{-3} N s/m^2, $\alpha_1=-6.6$, $\alpha_2=-77.0$, $\alpha_3=-4.2$, $\alpha_4=63.4$, $\alpha_5=62.4$, and $\alpha_6=-18.4$, and mass density $\rho=1021.5$ kg/m^3; and refractive indices for wavelength of light $\Lambda=670$ nm at 24.3 °C, $n_\parallel=1.708$ and $n_\perp=1.530$.

[1] J. L. Ericksen, Trans. Soc. Rheol. **5**, 23 (1961).
[2] F. M. Leslie, Arch. Ration. Mech. Anal. **28**, 265 (1968).
[3] P. G. de Gennes and J. Prost, *The Physics of Liquid Crystals* (Clarendon, Oxford, 1993); S. Chandrasekhar, *Liquid Crystals* (Cambridge University Press, Cambridge, 1992).
[4] F. M. Leslie, Adv. Liq. Cryst. **4**, 1 (1979).
[5] I. Zuniga and F. M. Leslie, Liq. Cryst. **5**, 725 (1989).
[6] I. Zuniga and F. M. Leslie, Europhys. Lett. **9**, 689 (1989).
[7] I. Zuniga and F. M. Leslie, J. Non-Newtonian Fluid Mech. **33**, 123 (1989).
[8] F. M. Leslie, in *Theory and Applications of Liquid Crystals*, edited by J. L. Ericksen and D. Kinderlehrer (Springer-Verlag, New York, 1987).
[9] E. Dubois-Violette and P. Manneville, in *Pattern Formation in Liquid Crystals*, edited by A. Buka and L. Kramer (Springer-Verlag, New York, 1996).
[10] P. Pieranski and E. Guyon, Solid State Commun. **13**, 435 (1973).
[11] P. Pieranski and E. Guyon, Phys. Rev. A **9**, 404 (1974).
[12] M. G. Clark, F. C. Saunders, I. A. Shanks, and F. M. Leslie, Mol. Cryst. Liq. Cryst. **70**, 195 (1981).
[13] W. R. Burghardt, J. Rheol. **35**, 49 (1991).
[14] A. P. Krekhov, L. Kramer, A. Buka, and A. N. Chuvirov, J. Phys. II **3**, 1387 (1993).
[15] A. P. Krekhov and L. Kramer, J. Phys. II **4**, 677 (1994).
[16] A. P. Krekhov and L. Kramer, Phys. Rev. E **53**, 4925 (1996).
[17] F. Scudieri, Appl. Phys. Lett. **29**, 398 (1976).
[18] F. Scudieri, J. Appl. Phys. **49**, 1289 (1978).
[19] E. Guazzelli, Thèse de 3me cycle, Chap. III.7, Université Paris–Sud, 1981 (unpublished).
[20] G. N. Belova and E. N. Remizova, Akust. Zh. **31**, 289 (1985) [Sov. Phys. Acoust. **31**, 171 (1985)].
[21] S. J. Hogan, T. Mullin, and P. Woodford, Proc. R. Soc. London, Ser. A **441**, 559 (1993).
[22] R. I. Linsey and S. J. Hogan (unpublished).
[23] E. N. Kozhevnikov, Zh. Éksp. Teor. Fiz. **91**, 1346 (1986) [Sov. Phys. JETP **64**, 793 (1986)].
[24] P. Pieranski and E. Guyon, Phys. Rev. Lett. **39**, 1280 (1977).
[25] E. Guazzelli and E. Guyon, J. Phys. (Paris) **43**, 985 (1982).
[26] E. Guazzelli, in *Nematics*, Vol. 332 of *NATO Advanced Study Institute Series B: Physics*, edited by Jean-Michel Coron, Jean-Michel Ghidaglia, and Frédéric Hélein (Kluwer, Dordrecht, 1991).
[27] E. Dubois-Violette and F. Rothen, J. Phys. (Paris) **39**, 1039 (1978).
[28] J. Sadik, F. Rothen, and W. Besgen, J. Phys. (Paris) **42**, 915 (1981).
[29] R. M. Clever and F. H. Busse, J. Fluid Mech. **65**, 625 (1974).
[30] S. Chandrasekhar, *Hydrodynamic and Hydromagnetic Stability* (Dover, New York, 1981).
[31] G. Ahlers, in *Pattern Formation in Liquid Crystals*, edited by A. Buka and L. Kramer (Springer-Verlag, New York, 1995).
[32] P. P. Karat and N. V. Madhusudana, Mol. Cryst. Liq. Cryst. **36**, 51 (1976).